12th International Conference on Computing and Control for the Water Industry, CCWI2013

Simulation of PID control applied to irrigation channels

A. Lacasta[a,*], M. Morales-Hernández[a], P. Brufau[a], P. García-Navarro[a]

[a]LIFTEC/EINA, University of Zaragoza. C/ María Luna 3, Zaragoza 50018, Spain

Abstract

Open-channel flow usually includes many hydraulic elements to help with the regulation of water supply in terms of automatic control. On the other hand, the one-dimensional Shallow Water Equations (SWE) are widely used to model and predict the flow dynamics in this kind of configurations. In this work, the unsteady SWE are used to model the water motion and they are solved using a finite volume upwind scheme able to cope with all flow regimes. Furthermore, the regulation of hydraulic structures at channels is frequently based on the PID controller. In this work, the implementation and coupling of the channel flow simulation with hydraulic elements and PID regulation is performed.

1. Introduction

On a global scale, the 70% of all fresh water is destined for irrigation purposes (UN, 2003). Extensive hydraulic structures to distribute the water and their regulation is required. In order to reduce water losses (Mareels et al., 2004). When dealing with automated channels, several implementations on the automation have been done such (Weyer (2002), Weyer (2003), Li et al. (2003), Ooi and Weyer (2003)). Moreover, one-dimensional hydraulic models have been demonstrated the proper indication for unsteady open-channel flow simulation (Burguete and García-Navarro, 2004). In this work, a decentralized feedback discrete PID controller have been implemented coupled with the hydraulic model in order to obtain a reliable complete simulation tool for predictive purposes. This may lead to PID calibrations for gate controller designers. Additionally, the implementation of the gates formulation has been compared with measured data obtained from the irrigation channel of Pina de Ebro (Zaragoza, SPAIN). This channel has been improved in the last years under an irrigation modernization plan has been applied. It is instrumented with water depth sensors and gate-opening recorders that help in the validation of the computational recreation of the scenarios. In order to stablish the stability of the PID implementation, the same case has been computationally regulated in order to verify the possibility to recreate the gate movement with an artificial PID controller. The use of PID lead to take a

---

* Corresponding author. Tel.: +34-876-846052

E-mail address: alacasta@unizar.es

first approach to the regulation problem providing us the possibility of applying more sophisticated techniques based on optimal control in the near future.

2. Governing equations

Free surface water in an irrigation channel can be modelled by the SWE which are a non linear partial derivative hyperbolic system of equations. This system can be derived from mass and momentum control volume analysis:

$$\frac{\partial \mathbf{U}(x,t)}{\partial t} + \frac{d\mathbf{F}(x,\mathbf{U})}{dx} = \mathbf{H}(x,\mathbf{U}) \tag{1}$$

$$\mathbf{U} = \begin{pmatrix} A \\ Q \end{pmatrix}, \quad \mathbf{F} = \begin{pmatrix} Q \\ \frac{Q^2}{A} + gI_1 \end{pmatrix}, \quad \mathbf{H} = \begin{pmatrix} 0 \\ g\left[I_2 + A\left(S_0 - S_f\right)\right] \end{pmatrix} \tag{2}$$

where Q is the discharge, A is the wetted cross section area, g is the acceleration due to the gravity, S_0 is the bed slope

$$S_0 = -\frac{\partial z}{\partial x} \tag{3}$$

where z is the bed level (See figure 1). S_f is the friction slope here represented by the empirical Manning law (Chow V.T. (1959))

$$S_f = \frac{Q^2 n^2}{A^2 R_h^{4/3}} \tag{4}$$

being R_h the hydraulic radius and n the Manning's roughness coefficient. I_1 represents a hydrostatic pressure force term

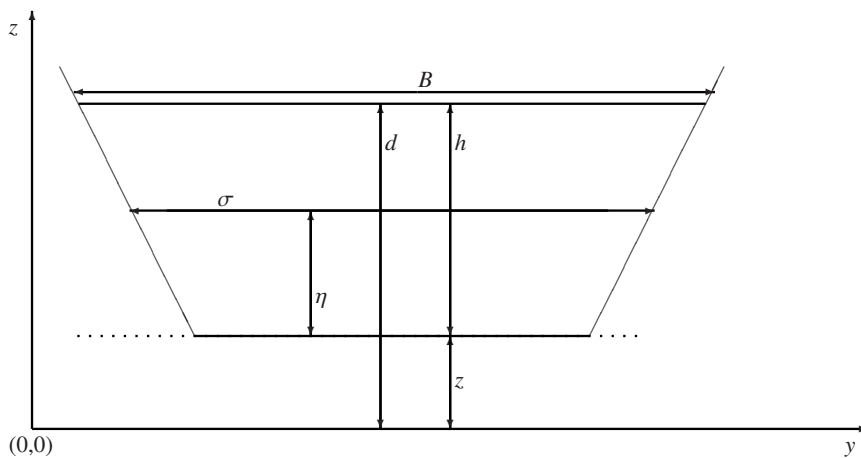$$I_1(x) = \int_0^h (h - \eta)\sigma(x,\eta)\, d\eta \tag{5}$$

Fig. 1: Coordinate system in a cross section as used in the 1D model

in a section of water depth $h = d - z$, water surface level d and width $\sigma(x,\eta)$ at a position η from the bottom (see Figure 1). Therefore, the cross sectional wet area can be expressed as follows:

$$A(x) = \int_0^h \sigma(x,\eta)\, d\eta \tag{6}$$

On the other hand, I_2 accounts for the pressure force due to the longitudinal width variations:

$$I_2(x) = \int_0^h (h - \eta)\frac{\partial\sigma(x,\eta)}{\partial x}\, d\eta \tag{7}$$

These equations don't have analytical solution in real geometry, so they have to be solved numerically by means of a numerical method.

3. Numerical scheme

It is possible to express equations (1) and (2) in a non-conservative form as in Burguete and García-Navarro (2001):

$$\frac{d\mathbf{F}(x,\mathbf{U})}{dx} = \frac{\partial\mathbf{F}(x,\mathbf{U})}{\partial x}\bigg|_{\mathbf{U}=const} + \frac{\partial\mathbf{F}(x,\mathbf{U})}{\partial\mathbf{U}}\bigg|_{x=const}\frac{\partial\mathbf{U}(x,t)}{\partial x} \tag{8}$$

Using (8), the 1D SWE (1) can be formulated as follows :

$$\frac{\partial\mathbf{U}(x,t)}{\partial t} + \mathbf{J}(x,\mathbf{U})\frac{\partial\mathbf{U}(x,t)}{\partial x} = \mathbf{H}'(x,\mathbf{U}) \tag{9}$$

being $H'(x,\mathbf{U})$ the vector related with the sources expressed in the non-conservative form:

$$\mathbf{H}'(x,\mathbf{U}) = \mathbf{H}(x,\mathbf{U}) - \frac{\partial\mathbf{F}(x,\mathbf{U})}{\partial x} \tag{10}$$

and $\mathbf{J}$ the Jacobian matrix of the original system

$$\mathbf{J} = \frac{\partial\mathbf{F}}{\partial\mathbf{U}} = \begin{pmatrix} 0 & 1 \\ c^2 - u^2 & 2u \end{pmatrix} \tag{11}$$

with $u = Q/A$ and $c = \sqrt{gA/B}$ (B is the top width at the free surface) (See Figure 1).
Following the Leibnitz rule, it is possible to express the link between I_1 and I_2 in this manner Cunge et al. (1989):

$$\frac{\partial I_1}{\partial x} = I_2 + A\frac{\partial h}{\partial x} \tag{12}$$

As stated in Morales-Hernández et al. (2013b), the total derivatives account for the pure spatial variations in x. Moreover, it is worth remarking the difference between the partial and the total derivatives when discretizing the equation: the discrete increments approach actually the total derivatives and not the partial derivatives. Therefore, all terms have to be carefully expressed in total derivatives. In particular:

$$\frac{dh}{dx} = \frac{\partial h}{\partial x} + \frac{\partial h}{\partial A}\frac{\partial A}{\partial x} = \frac{\partial h}{\partial x} + \frac{1}{B}\frac{\partial A}{\partial x} \tag{13}$$

From (12) and (13), the non-conservative source term is expressed as follows:

$$\mathbf{H}'(x,\mathbf{U}) = \mathbf{H}(x,\mathbf{U}) - \frac{\partial\mathbf{F}(x,\mathbf{U})}{\partial x} = \begin{pmatrix} 0 \\ gA\left(S_0 - S_f - \frac{dh}{dx} + \frac{1}{B}\frac{dA}{dx}\right) \end{pmatrix} \tag{14}$$

where the equivalence between the partial and total x-derivatives of the conserved variable A should be noted. The Jacobian matrix (11) can be diagonalized

$$\mathbf{J} = \mathbf{P\Lambda P}^{-1}, \quad \mathbf{\Lambda} = \mathbf{P}^{-1}\mathbf{J}\mathbf{P} \tag{15}$$

where the diagonal matrix $\mathbf{\Lambda}$ is formed by the eigenvalues of $\mathbf{J}$, and $\mathbf{P}$ is constructed with its eigenvectors.

$$
\mathbf{P} = \begin{pmatrix} 1 & 1 \\ \lambda_1 & \lambda_2 \end{pmatrix}, \quad \mathbf{\Lambda} = \begin{pmatrix} \lambda_1 & 0 \\ 0 & \lambda_2 \end{pmatrix},
$$

$$
\mathbf{e}_k = \begin{pmatrix} 1 \\ \lambda_k \end{pmatrix}, \quad \lambda_1 = u - c, \quad \lambda_2 = u + c
\tag{16}
$$

The equations in non-conservative form can be discretized in a regular mesh by means of the first order explicit scheme. Roe's linearization (Roe, 1981) allows to express the differences in the conserved variables and in the source terms across the grid edge $i + 1/2$ as a sum of waves:

$$
\delta\mathbf{U}_{i+1/2} = \mathbf{U}_{i+1} - \mathbf{U}_i = \sum_{m=1}^{2} (\tilde{\alpha}_m\, \tilde{\mathbf{e}}_m)_{i+1/2},
$$

$$
(\tilde{\mathbf{H}}'\, \delta x)_{i+1/2} = \sum_{m=1}^{2} (\tilde{\beta}_m\, \tilde{\mathbf{e}}_m)_{i+1/2}
\tag{17}
$$

with

$$
\tilde{\lambda}_1 = \tilde{u} - \tilde{c}, \quad \tilde{\lambda}_2 = \tilde{u} + \tilde{c}, \quad \tilde{\alpha}_1 = \frac{\tilde{\lambda}_2\, \delta A - \delta Q}{2\tilde{c}}, \quad \tilde{\alpha}_2 = \frac{-\tilde{\lambda}_1\, \delta A + \delta Q}{2\tilde{c}},
$$

$$
\tilde{\beta}_1 = -\frac{1}{2\tilde{c}} \left\{ g\tilde{A} \left[(\tilde{S}_0 - \tilde{S}_f)\delta x - \delta h + \frac{1}{\tilde{B}}\delta A \right] \right\}, \quad \tilde{\beta}_2 = -\tilde{\beta}_1,
\tag{18}
$$

$$
\tilde{u}_{i+1/2} = \frac{\sqrt{A_i}u_i + \sqrt{A_{i+1}}u_{i+1}}{\sqrt{A_i} + \sqrt{A_{i+1}}}, \quad \tilde{c}_{i+1/2} = \sqrt{g\frac{A_i + A_{i+1}}{B_i + B_{i+1}}}
$$

where the tilde variables represent an average state at each edge. The entropy fix can be found in Murillo and García-Navarro (2010). The contributions due to the fluxes and the source terms can be expressed in a compact formulation as follows:

$$
\tilde{\gamma}^{\pm}_{i+1/2} = \left(\frac{1}{2} \left[1 \pm \text{sign}\left(\tilde{\lambda}\right) \right] \tilde{\gamma} \right)_{i+1/2}
\tag{19}
$$

where

$$
\tilde{\gamma}_{i+1/2} = \left(\tilde{\lambda}\, \tilde{\alpha} - \tilde{\beta} \right)_{i+1/2}
\tag{20}
$$

Therefore, the first order explicit upwind numerical scheme is formulated as follows:

$$
\Delta\mathbf{U}_i^n = -\frac{\Delta t}{\delta x} \left[\sum_m (\tilde{\gamma}_m^+\, \tilde{\mathbf{e}}_m)_{i-1/2} + \sum_m (\tilde{\gamma}_m^-\, \tilde{\mathbf{e}}_m)_{i+1/2} \right]^n = -\frac{\Delta t}{\delta x} \left[\delta\mathbf{M}_{i-1/2}^+ + \delta\mathbf{M}_{i+1/2}^- \right]^n
\tag{21}
$$

It illustrates that the in-going contributions from left and right walls are used to update the value of the conserved variables at every cell. The scheme so built has been proved to be robust, conservative, well-balanced and positivity preserving Burguete and García-Navarro (2004).

The most usual physical boundary conditions at the inlet are hydrograph $Q(t)$ or water depth $h(t)$. Both $\{Q(t), h(t)\}$ are required to impose supercritical flow. Outlet conditions are usually $h(t)$ or a rating curve $Q(h)$. Numerical boundary conditions consist of imposing to the first and last cells A or Q. The other variable will internally computed using

$\delta \mathbf{M}_{i+1/2}^{-}$ and $\delta \mathbf{M}_{i-1/2}^{+}$ respectively.

The time step Δt is dynamically chosen following this expression

$$\Delta t = \text{CFL} \ \min_{i,m} \left(\frac{\delta x}{|\tilde{\lambda}_m|_i^n} \right), \qquad \text{CFL} \le 1 \tag{22}$$

where CFL is the Courant-Friedrich-Lewy number.

4. Gates modeling

4.1. Mathematical modeling

Gates are modeled following Morales-Hernández et al. (2013a) by assuming that the discharge per unit breadth q crossing the gate is governed by the difference between the water surface level ($d = h + z$) on both sides of the gate, referred to as d_l upstream of the gate and d_r downstream of the gate, and by the allowable gate opening, G_o. Several situations are envisaged. In the case that $G_o = 0$ the gate behaves as a solid wall and no flow crosses the gate. When the gate opening is larger than the surface water level on both sides, it no longer influences the flow. In any other case, assuming that $d_l < d_r$, without lost of generality, two different flow situations can occur depending on the relative values of G_o, z_l, z_r, d_l and d_r. When $G_o + max(z_l, z_r) < min(d_l, d_r)$, Figure 2a, the discharge is given by

$$Q = BG_oK_1(d_r - d_l)^{1/2} \tag{23}$$

with K_1 an energy loss coefficient. In this work $K_1 = 3.33$ (Henderson (1966)).

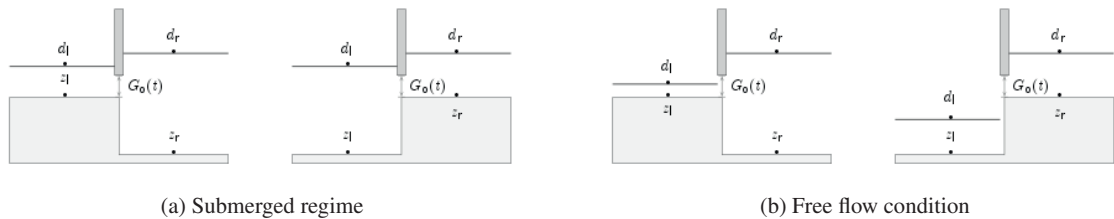(a) Submerged regime   (b) Free flow condition

Fig. 2: Water levels for submerged conditions (a) and for free flow conditions (b)

When $G_o + max(z_l, z_r) > min(d_l, d_r)$, Figure 2b, the discharge is given by

$$Q = BG_oK_2(d_r - max(z_l, z_r))^{1/2} \tag{24}$$

with K_2 another energy loss coefficient. In this work $K_2 = 2.25$ (Henderson (1966)).

4.2. Numerical modeling

In order to simulate cross structures, non-linear algebraic equations must be combined with flow numerical modelling. Following Morales-Hernández et al. (2013a) the flow through a gate, a special case of internal boundary condition, is associated with an edge $k = \{l, r\}$ defined between cells l and r. Gate edge either stop the flow (solid wall), or allow free surface flow and pressurized flow. Pairs of cells associated with a gate edge are referred to as gate cells. Depending on the flow conditions and the gate management operation four cases can be defined:

- If the gate opening level is above both surface levels, $G_o + max(z_l, z_r) > max(d_l, d_r)$, the flow will be considered as free surface flow and the gate cells (l, r) are updated as ordinary cells using (21).

- If the gate is closed, $G_o = 0$, the associated gate edge k_{gate} is a solid wall, with a zero velocity component. As there are no contributions from the gate edge, $\delta \mathbf{M}_k = 0$ is set in (21) when updating the conserved values in the gate cells (l, r) at time level $n + 1$.
- When the gate opening is smaller than the free surface of either gate cell, $G_o + max(z_l, z_r) < min(d_l, d_r)$ the flow is assumed pressurized. The discharge is computed using (23) and imposed in both cells (l, r). Moreover, in this case $\delta \mathbf{M}_k = 0$ is imposed at the gate edge.
- Otherwise, the gate discharge is computed using (24) and imposed in both cells (l, r). Also, in this case $\delta \mathbf{M}_k = 0$ is imposed at the gate edge.

For either the closed gate or pressurized flow, the variation of the water depth at the gate cells (l, r) is a result of contributions from neighbouring cells, ensuring exact mass conservation.

Lateral gates are formulated as cross gates but considering only free-flow conditions. For lateral gates, calculated Q is integrated along the time-step and then, the water volume is extracted from the involved cell. This allows to satisfy the free flow condition that depends just on the upstream water depth and gate opening, and emulates what the numerical method applies for the gate edge.

5. Gates formulation validation

The model has been tested using a real irrigation channel located in Pina de Ebro (Zaragoza) at North-East of Spain. The irrigation channel has a total length of 12334 m with variable bed-slope and constant section of height 1.8 m and width 2.5 m.
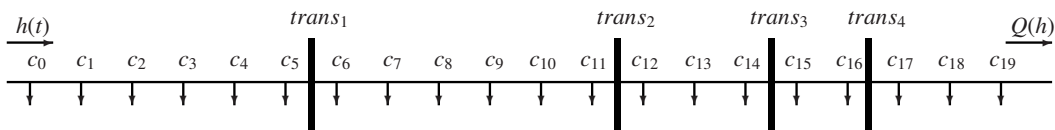

Fig. 3: Representation of the channel. $c_{\{1..19\}}$ show the location of the lateral gates and $trans_{\{1..4\}}$ the position of the cross gates.

The channel contains 4 cross gates and 19 lateral gates. The cross gates are instrumented with data loggers which records the gate displacement each 10 minutes. Moreover, the lateral gates record their state as open or not with constant opening (Figure 4). The lateral gates are connected with secondary $r = 300 mm$ pipes. So that the discharge conditions can be considered as free flow. Taking this into account and considering the lateral outlet as square, the outlet width b is such that $A = bG_0 = \pi r^2$ being G_0 the lateral gate opening. Figure 4 shows the time evolution of the lateral gate openings for the simulated period. Gate 18 is open the whole simulation and gate 19 and 16 are closed all the time.
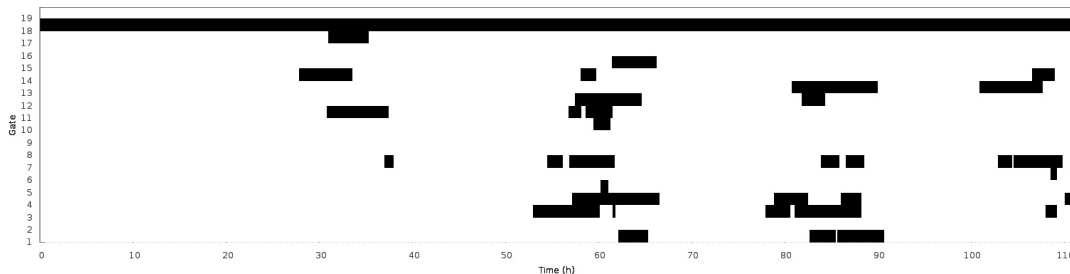

Fig. 4: Lateral gates opening. Dark areas represents time intervals where lateral gate is open.

In this case, the model is used to reproduce reproduces the behavior of the channel during 120 hours between 01/01/12 and 01/05/12. The movement of the gates is applied as data loggers registered. The data were got with 10 minutes period. In the first case, it was assumed that no movement took place during this time. This assumption does not allow the simulation to capture the continuous behavior of the gate dynamics. The inlet depth measured upstream c_1 is applied as inlet condition and the gauge curve calibrated at the end of the channel is used as outlet boundary condition. The numerical initial condition is dry bed.
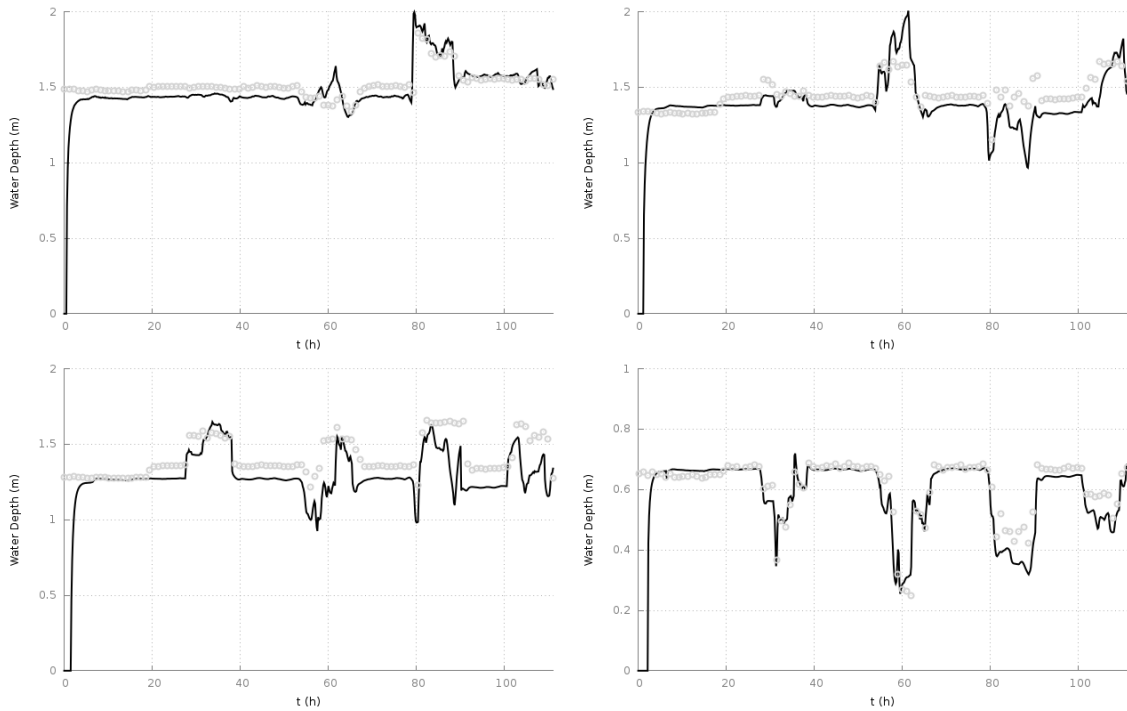

Fig. 5: Right-Left, Top-Down, results for simulated ($-$) and measured ($\circ$) water depth between 01/01/12 and 01/05/12 upstream first, second and third cross gate and at the end of the channel.

Figure 5 shows the results of the time evolution at cross gates 1,2 and 3, and at the end of the channel for the simulated period. Until $t \approx 1h$. the proper pseudo-steady state has not been reached. A good agreement between simulated and measured water depth can be observed. Some differences appear at the third cross gate where lateral discharges are very variable. It means that between 80-90 hours several lateral discharges appear (See figure 4) . When analyzing gate openings, some suspicious glitches are recorded and these may introduce perturbations that may lead to strong variations on the water depth in the measured point.

6. PID Controller

6.1. PID algorithm

The PID algorithm is the best known feedback controller used within the process industries (Bernett, 1993). It has been successfully used for over 50 years. It is a robust well understood algorithm that can provide control according to the value of an error signal produced as the difference between a real level and a setpoint level.

The equation of the PID controller can be formulated as a function of time as follows:

$$u(t) = K\left(e(t) + \frac{1}{T_i}\int_0^t e(\tau)d\tau + T_d\frac{de(t)}{dt}\right) = P + I + D \tag{25}$$

where u is the controller action, in this case the gate opening, and e is called the control error ($e = y_{ref} - y$) where y_{ref} is the *setpoint*, in our case the water depth, y is the measured variable and τ is the variable of integration (time in the present case). The constant K defines the gate position according to the difference between the setpoint and the real level; T_i is related to the data length of the error signal; T_d defines the gate reaction to the current changes in the error signal.

6.2. Numerical modeling

The discrete representation of (25) for the gate regulation is as follows:

$$u(t_k) = K\ e(t_k) + \frac{K\ T_s}{T_i}\sum_{i=0}^{t_k} e(i) + \frac{KT_d\ (e(t_k) - e(t_{k-1}))}{T_s} \tag{26}$$

where T_s is the sampling time (understood as the time in which the controller provides a new gate position) and t_k is the current time. After writing (26) in terms of time increments, the discrete representation of the PID equations is:

$$u(t_k) = u(t_{k-1}) + \underbrace{K\left(1 + \frac{T_s}{T_i} + \frac{T_d}{T_s}\right)\left(y(t_k) - y_{ref}\right)}_{f(t_k)} - \underbrace{K\left(1 + \frac{2T_d}{T_s}\right)\left(y(t_{k-1}) - y_{ref}\right)}_{f(t_{k-1})} + \underbrace{K\frac{T_d}{T_s}\left(y(t_{k-2}) - y_{ref}\right)}_{f(t_{k-2})} \tag{27}$$

where y_{ref} is the setpoint or target value for the controlled variable and y is the current value of the controlled variable. This algorithm is completely incorporated into the hydraulic numerical scheme (21), providing a new position of the gate when necessary. Additionally, some weights could be applied to $f(t_k), f(t_{k-1}), f(t_{k-2})$ to make more stable the PID. This coefficients will be labeled as $\alpha_1, \alpha_2, \alpha_3$ and they take values between 0 and 1.

7. Results for PID controller

The second case uses the PID formulation to regulate the movements of the cross gates in order to preserve a target water level upstream the gates but considering the lateral gates with the same movements in the first case. The target level at each gate will be the measured level in order to analyze how can the PID fit to a real data set. The configuration of the PID will be predefined as in Table 1 following Morales-Hernández et al. (2013a). Additionally, the V_{max} models the maximum displacement for the gate, associated to the gate engine.

Table 1: PID tuning parameters for Case 2

α_1	α_2	α_3	K_s	T_i	T_d	T_s	V_{max}
1.0	0.8	0.6	1.0	30.0	0.8	1.0	0.009

This case shows that the PID formulation gets the desired level highlighting the profits of using this technique to calibrate the PID controllers for open-channel flows. Results (Figure 6) show that this configuration of PID controllers captures adequately the unsteady phenomena and provides the correct gate movements to obtain the desired water levels. In this case, the third gate obtains the same upstream water level. The main reason is that gate uncertainty in the formulation leads to more sensitive water depth prediction. In this case, when using the PID formulation, the water level is the variable which drives the gate movement and, because of this, the gate movement is not as discrete as in the first case. This is the key of the fitting to the measurements.
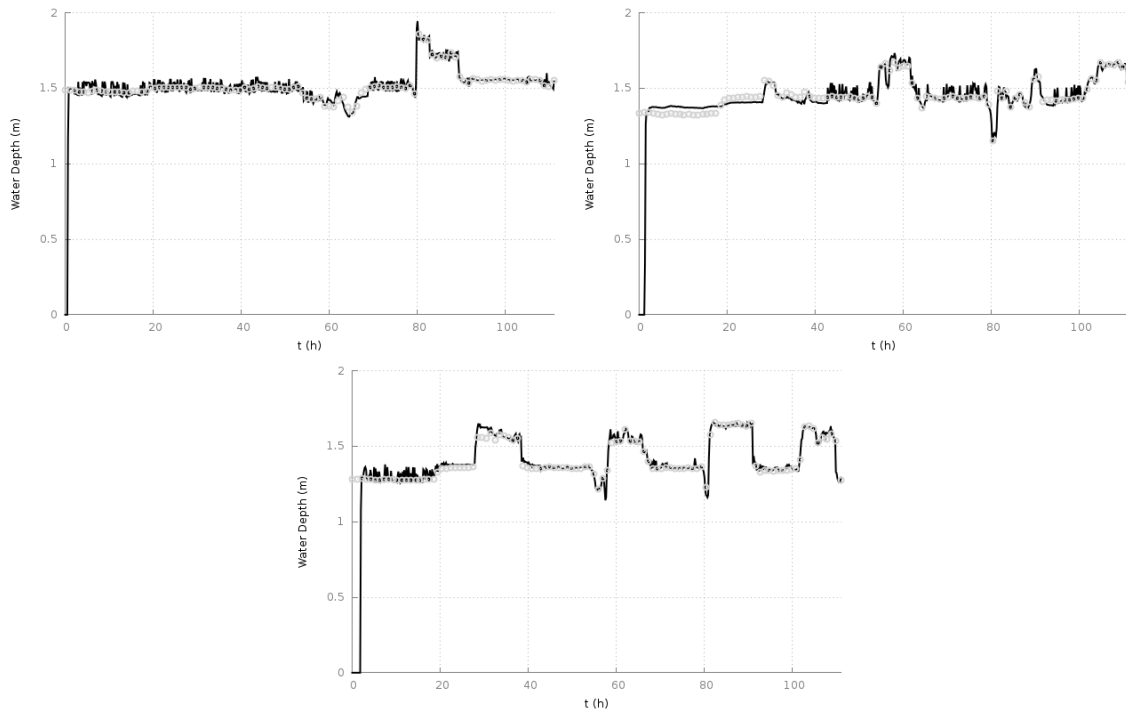
Fig. 6: Right-Left, Top-Down, results for regulated (−) and measured (◦) water depth between 01/01/12 and 01/05/12 at upstream first, second and third cross gate.

Conclusions

In this work, a numerical model for irrigation channel simulation has been formulated. The model is based on an upwind finite volume scheme and includes the formulation of lateral gates and cross gates coupled with PID regulation. The model has been tested with a real irrigation channel and validated with a 5 days period of gate operations within the channel. Moreover, the numerical simulation of the PID has been explored in order to obtain the same behavior that the flow shows along time. The results indicate a good agreement between simulated and measured data. The complexity of the operations and the influence in the channel flux have been captured by both, simulated and regulated cases. The validation of this formulation may allow to use this model as a predictive tool for PID tests.

Acknowledgments

References

The United Nations World Water Development Report, *executive summary. 2003*

I. Mareels and E. Weyer. Systems engineering for irrigation systems. In Proc. 10th IFAC/IFORS/IMACS/IFIP Symposium on Large Scale Systems, pages 3240, Osaka, Japan, 2004.

E. Weyer. Decentralised PI control of an open water channel. In Proc. 15th IFAC World Congress, Barcelona, Spain, July 2002.

E. Weyer. LQ control of an irrigation channel. In Proc. of the 42nd IEEE CDC, pages 750755, 2003.

Y. Li, M. Cantoni, and E. Weyer. Design of a centralised controller for the Haughton Main Channel using H loop-shaping. In Proc. UKACC Control Conf., Bath, UK, 2004.

S.K. Ooi and E. Weyer. Control design for an irrigation channel from physical data. In Proc. of the 2003 Euro. Cntrl. Conf., Cambridge, UK, 2003.

J. Burguete and P. García-Navarro, Improving simple explicit methods for unsteady open channel and river flow International Journal for Numerical Methods in Fluids, 45, 125–156. (2004)

Ven Te Chow, Open-Channel Hydraulics. McGraw-Hill, (1959)

J. Burguete and P. García-Navarro, Efficient construction of high-resolution TVD conservative schemes for equations with source terms: application to shallow water flows, International Journal for Numerical Methods in Fluids, 37, 209–248. (2001)

J.A. Cunge, F.M. Holly, A. Verwey, Practical aspects of computational river hydraulics. Pitman Pub Inc. (1989)

P.L. Roe, Approximate Riemann solvers, parameter vectors and difference schemes, Journal of Computational Physics, 43, 357–372. (1981)

J. Murillo and P. García-Navarro, Weak solutions for partial differential equations with source terms: Application to the shallow water equations, J. Comput. Phys. 229 4327–4368. (2010)

M. Morales-Hernndez, P. Garca-Navarro, J. Burguete, P. Brufau, A conservative strategy to couple 1D and 2D models for shallow water flow simulation, Computers & Fluids, Volume 81, Pages 26-44 (2013a)

M. Morales-Hernández, P. García-Navarro and J. Murillo, The formulation of internal boundary conditions in unsteady 2-D shallow water flows: application to flood regulation, Water Resour. Res., 49, (2013b)

Henderson, F.M.(1966) Open Channel Flow *MacMillan series in civil Engineering*

Bennett, S., "Development of the PID controller," Control Systems, IEEE , vol.13, no.6, pp.58,62, (1993)